Ultra Sensitive Label-Free Detection of Biomolecules Using Vertically Extended Drain Double Gate $Si_{0.5}Ge_{0.5}$ Source Tunnel FET

Kumari Nibha Priyadarshani and Sangeeta Singh, *Member, IEEE*

***Abstract*— This work reports a vertically extended drain double gate $Si_{0.5}Ge_{0.5}$ source tunnel FET for the biomolecules detection using its electrical properties modulation in presence of biomolecules like cell, DNA, protein, etc. The reported biosensor has a dual source of $Si_{0.5}Ge_{0.5}$ and two cavities above each source-channel interface for the immobilization of biomolecules. This immobilization modulates the screening/tunneling length and energy range available for tunneling due to the dielectric constant and charge density variations of the biomolecules. The dual cavity structure increases the control of biomolecules on the source to channel tunneling probability and thus realizes an increased control on electrical performance parameters of the biosensor enabling it to have a higher sensitivity towards the biomolecules. Further, the cavity length of the reported biosensor is kept as 45 nm making it suitable for large sized biomolecules and polymers detection also. Our study demonstrates that the reported biosensor structure is resilient towards the process variations and temperature effects. Moreover, the effect of dielectric modulation and charge density modulation has also been analyzed in terms of the variation in the drive current, ON state current, threshold voltage, transconductance, and sub-threshold slope (SS). The sensitivity of the reported biosensor is also compared with the existing biosensors and it is found to be highly sensitive.**

***Index Terms*— Biosensor, ultra-sensitive, tunnel FET, $Si_{0.5}Ge_{0.5}$ source, vertically extended drain double gate, sub-threshold slope (SS).**

I. Introduction

THE electrical properties of biological molecules make them suitable for their label-free electrical detection by deploying field effect transistors. Several biological molecules detectors have made the life of people convenient such as blood glucose monitoring etc. This introduces a strong need for biosensors for society that too in the current pandemic situations. Reduction in the feature size of the transistor has led to different short channel effects (SCEs) which gradually deteriorates the device performance. Tunnel FET overcomes this limitation of CMOS transistor owing to its charge carrier tunneling from source to channel [1]–[3]. Further, it is immune to SCEs, overcomes the threshold voltage limitation of subthreshold slope (SS) unlike CMOS devices [4], [5]. It provides a steep subthreshold slope (SS), low OFF state current, high I_{ON}/I_{OFF} ratio despite low ON state current [6], [7]. Ambipolar current is another disadvantage of TFET devices [8]–[10]. Vertical TFETs suppress the ambipolar current as well as enhance drive current because of the controllable channel-drain screening length as reported in [11], [12]. The electrical performance parameters of the TFETs demonstrates huge performance variation with respect to the dielectric constant of the gate dielectric and interface trap charges. This modulation of electrical parameters can be deployed for realizing a biosensor [13].

P. Bergveld firstly designed and investigated a biosensor for neurophysiological measurements, and it was ion-sensitive FET (ISFET) [14]. ISFET demonstrated good sensitivity for the charged biomolecules, on the other hand the sensitivity for the neutral biomolecules was low and is also not compatible with the CMOS process. Hence, dielectrically modulated field effect transistors (DM-FETs) are deployed for the electrical detection of the neutral biomolecules and they are CMOS process compatible also [15], [16]. Nevertheless, DM-FETs are hindered by various shortcomings of conventional FET structures like drain induced barrier lowering (DIBL) and many more SCEs. Hence, the electrical parameters of DMFETs get deteriorated due to the increase in power consumption, higher biomolecule detection time, and lesser sensitivity [17]. Thus the dielectrically modulated tunnel field effect transistors (DM-TFETs) [18]–[20] have been broadly utilized for the label-free detection of biomolecules owing to its inherent structural advantages such as ultra-low power operation, better sensitivity, better response time, energy-efficient because of low leakage, the potential to tame different demerits of FET based sensors [21], [22]. Recently, various other device structures are reported for the biosensing applications [23]–[25].

In this present work, we deployed the vertically extended drain double gate $Si_{0.5}Ge_{0.5}$ source tunnel FET (VD-DG-$Si_{0.5}Ge_{0.5}$S-TFET) for label-free electrical detection

Manuscript received April 5, 2021; revised July 28, 2021; accepted August 14, 2021. Date of publication August 23, 2021; date of current version October 1, 2021. *(Corresponding author: Sangeeta Singh.)*

The authors are with the Microelectronics and VLSI Design Laboratory, Department of Electronics and Communication Engineering, National Institute of Technology Patna, Patna 800005, India (e-mail: nibha@nitp.ac.in; sangeeta.singh@nitp.ac.in).

Digital Object Identifier 10.1109/TNB.2021.3106333

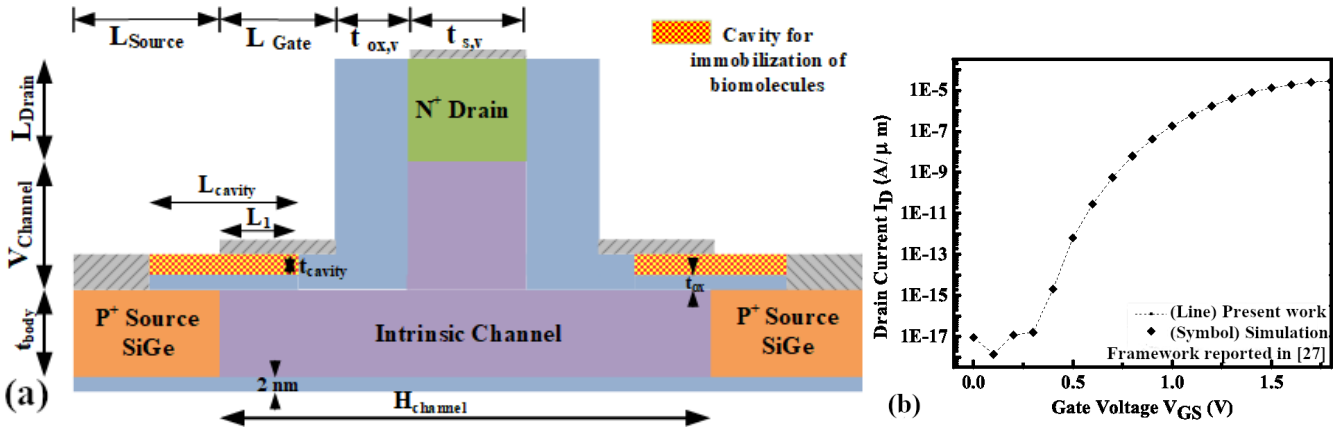

Fig. 1. (a) Reported vertically extended drain double gate $Si_{0.5}Ge_{0.5}$ source tunnel FET based biosensor and (b) transfer characteristics of the simulation framework calibration with respect to the double gate TFET structure reported in [27].

of biomolecules like cells, enzymes, DNA, proteins, etc. VD-DG-$Si_{0.5}Ge_{0.5}$S-TFET shows a higher drive current as compared to drain engineered quadruple gate TFET (DE-QG-TFET) as reported in our earlier literature [11]. The reported biosensor VD-DG-$Si_{0.5}Ge_{0.5}$S-TFET device structure has a dual source channel junction and vertical drain. To make the device structure biosensor a nanogap is embedded in the gate oxide region by etching away the sacrificial layer for the immobilization of the biomolecules. This novel device structure allows biomolecules immobilization in both the cavities above source channel junction to regulate the tunneling length and energy range available for tunneling at both the junctions thus having higher control on tunneling probability, making it highly sensitive to biomolecules. Further, the cavity length is 45 nm allows the device to sense larger biomolecules and polymers as well. Our work analyses the sensor characteristics variation with variation in the biomolecule dielectric constant as well as the charge density. The impact of cavity thickness variation on the sensitivity of biosensor has also been analyzed here. Further, the impact of biomolecule occupancy level in nanocavity on drain current has also been analyzed.

This work is organized as follows: Section II explains device structural parameters, material and doping. Section III analyzes the effect of cavity thickness variation on the biosensor sensitivity, sensitivity variation with dielectric modulation and charge density modulation, and impact of biomolecule occupancy in embedded nanocavity on drain current. Further, section IV concludes our exhaustive analysis of the biosensor.

II. Device Structure and Simulation Models

A 2D cross-sectional view of the considered vertically extended drain double gate $Si_{0.5}Ge_{0.5}$ source tunnel FET (VD-DG-$Si_{0.5}Ge_{0.5}$S-TFET) is shown in Fig. 1 (a). The channel is reverse T shaped with two sources at the two ends of the horizontal channel and a drain at the top of the vertical channel with a double gate on the horizontal channel. The drain and channel regions are of silicon with n-type doping of $1 \times 10^{17} cm^{-3}$ for the channel region and $5 \times 10^{18} cm^{-3}$ for the drain region. The source is of p-type doping of the order of $1 \times 10^{20} cm^{-3}$ composed of strained silicon ($Si_{0.5}Ge_{0.5}$) to increase the ON current. The oxide used here is $Si\,O_2$. Due to the binding of biomolecules in the sensing embedded nanocavity regions, there will be a modulation in device electrical performance parameters such as drive current, threshold voltage, maximum transconductance, SS, etc. This changes are calibrated to sense the biomolecules. Further, device parameters considered during the device emulations are tabulated in Table. I. The gate oxide has been etched to form a cavity for the immobilization of biomolecules under both gates. As the drain is on the vertical channel it provides independent tuning of source-channel and channel-drain interface. Moreover, gate oxide and vertical oxide thickness can also be tuned independently that enables a good control to suppress ambipolar current as well as enhances the drive current.

TABLE I
Device Parameters for VD-DG-$Si_{0.5}Ge_{0.5}$S-TFET Based Biosensor

Parameters	Symbols	Values (unit)
Body thickness	t_{body}	10 nm
Channel length	$H_{channel}$	105 nm
vertical channel thickness	$t_{s,v}$	25 nm
vertical channel length	$V_{channel}$	35 nm
oxide thickness under cavity	t_{ox}	0.5 nm
vertical oxide thickness	$t_{ox,v}$	15 nm
Cavity thickness	t_{cavity}	2.5 nm-5.5 nm
Cavity Length	L_{cavity}	45 nm
Cavity under gate	L_1	20 nm
Gate length	L_G	25 nm
Gate workfunction	φ_{Gate}	4.5 eV
Source length	L_{source}	50 nm
Drain length	L_{drain}	15 nm

The analysis has been done by using ATLAS TCAD Silvaco tool [26]. Here, the non-local band-to-band tunneling model has been incorporated for the precise modeling as it includes the spatial profile of energy band and spatial distribution of electrons and holes in conduction and valence bands, respectively. SRH and Auger recombination models have also been included for considering the generation and recombination of carriers. Concentration-dependent and field dependent mobility models have been considered along with trap assisted tunneling, band gap narrowing, and drift diffusion transport models. The simulation framework deployed here for the analysis of VD-DG-$Si_{0.5}Ge_{0.5}$S-TFET biosensor is

exhaustively calibrated with the data reported in [27] as shown in Fig. 1 (b). As [27] is already calibrated with the experimental data for the fabricated IBM tunnel diode as reported in [28], hence the authors have calibrated their simulation frame work against [27]. The tunneling current can be mathematically expressed as [11]:

$$I_{tunn} \propto T(E) \cong exp\left[-\frac{4\sqrt{2m^*}E_g^{\frac{3}{2}}}{3q\hbar(E_g+\Delta\Phi)}\sqrt{\frac{\varepsilon_{Si}}{\varepsilon_{bio}}t_{oxt}t_{body}}\right]\Delta\Phi \quad (1)$$

$$\lambda = \sqrt{\frac{\varepsilon_{Si}}{\varepsilon_{bio}}t_{oxt}t_{body}} \quad (2)$$

where, I_{tunn} is the tunneling current, $T(E)$ stands for the probability of tunneling, m^* is the effective mass of carrier, E_g is the energy bandgap at the tunneling junction, $\Delta\Phi$ is the energy range available over which tunneling of charge carrier can occur, and $t_{oxt} = t_{ox} + t_{cavity}$ is the thickness of oxide and cavity under gate, t_{body} is the body thickness, ε_{bio} dielectric constant of immobilized biomolecules, and ε_{Si} is the dielectric constant of channel semiconductor, and λ is screening/tunneling length.

This VD-DG-$Si_{0.5}Ge_{0.5}$S-TFET structure can be realized by following the similar the fabrication process technology as reported in [9]. Thin silicon film can be taken to act as the channel region and etched to form source region. Epitaxial growth of SiGe layer in the etched region to from source region and for the P^+ realization of dual sources ion implantation can be deployed. Now, layer of oxide can be grown and then it can be selectively etched for the formation of vertical channel and drain. It will define seed window for the epitaxial growth of silicon. Further, N^+ drain formation can be done by ion implantation, followed by selective etching of oxide to form gate oxides. Finally, metallization for source, drain and gate contacts can be done. Further, now-a-days the state-of-art of the silicon technology has empowered epitaxial growth of high quality SiGe layer without any defect [29], [30]. To concentrate Ge concentration while oxidation of SiGe layer, the condensation technique has been successfully reported [30], [31]. Moreover, the realization of hetero bandgap can be done by local oxidation of SiGe layer [32], [33].

III. Result and Discussion

A. Cavity Thickness Variation With $\kappa = 4$

The dielectric constant of various biomolecules like biotin ($\kappa = 2.63$), uricase ($\kappa = 1.54$), protein ($\kappa = 2.50$), amino propyl triethoxysilane ($\kappa = 3.57$), etc. are reported in [22], [34]–[36]. This dielectric constant of the biomolecules can be utilized here to detect them using VD-DG-$Si_{0.5}Ge_{0.5}$S-TFET device structure. Here, biosensor analysis has been done for dielectric constant variation up to $\kappa = 10$. The effects of cavity thickness variation with $\kappa = 4$ on the potential and energy band under oxide-silicon interface have been shown in Fig. 2 (a) and (b), respectively. With an increase in cavity thickness the potential drop across the gate capacitance increases and thus the potential under oxide-silicon interface decreases as in Fig. 2 (a). This decrease in potential with an

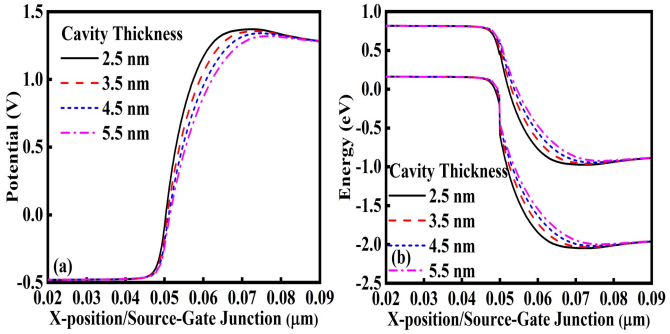

Fig. 2. (a) Potential and (b) energy band at source-gate junction 1 nm below oxide-silicon interface with variation in cavity thickness in ON state ($V_{DS} = 1$ V; $V_{GS} = 2$ V) and $\kappa = 4$.

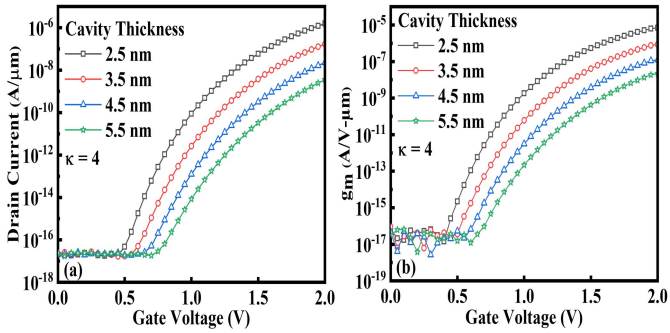

Fig. 3. (a) Transfer characteristics and (b) transconductance of the biosensor with variation in the cavity thickness at $V_{DS} = 1$ V and $\kappa = 4$.

increase in cavity thickness shifts the energy band upwards as indicated in Fig. 2 (b), which leads to rise in the tunneling barrier and degradation in the tunneling probability. This decrease in tunneling probability can also be depicted from equation (1) and (2) where an increase in the t_{cavity}/t_{oxt} will lead to rise in the screening length and thus decline in the tunneling probability $T(E)$. Fig. 3 (a) shows the transfer characteristics of considered biosensor with variation in cavity thickness available for immobilization of biomolecules with dielectric constant, $\kappa = 4$ and $V_{DS} = 1$ V. With enhancement in the thickness of cavity the gate control is reduced and the energy band in the channel region shifts upwards leading to rise in the tunneling length and thus a decrease in the tunneling probability/drive current as evident from equations (1) and (2). Thus, the maximum drive current is obtained for the cavity thickness of 2.5 nm. Fig. 3 (b) shows the transconductance of the reported biosensor with variation in the cavity thickness and dielectric constant of biomolecule as $\kappa = 4$. Transconductance also increases with a decrease in the cavity thickness and maximum transconductance is achieved for the cavity thickness of 2.5 nm.

Further, Fig. 4 (a), (b), (c), and (d) show the sensitivity of biosensor with cavity thickness variation for the different dielectric constants of the biomolecules with reference to air in the cavity. Sensitivity is defined in terms of ΔI_{ON}, ΔV_{TH}, Δg_m, and SS computed as,

$$\Delta I_{ON} = \left| I_{ON,\kappa} - I_{ON,air} \right| \quad (3)$$

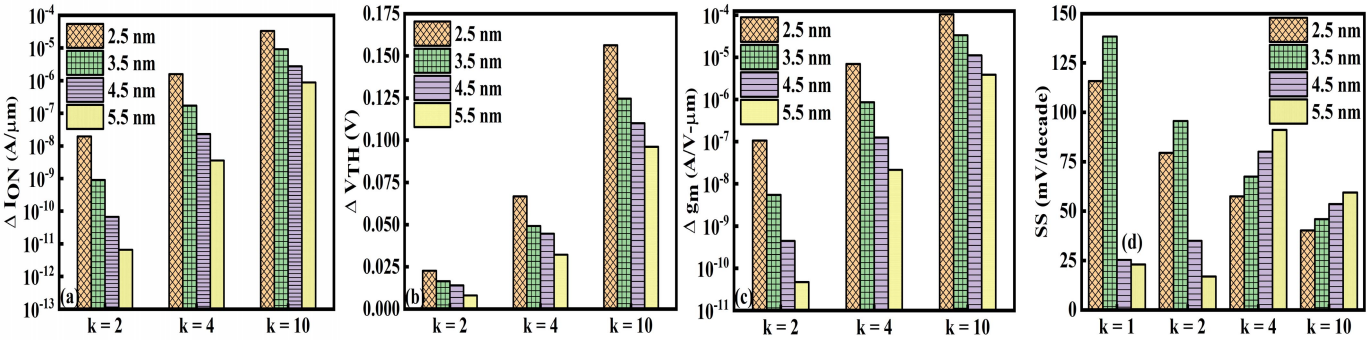

Fig. 4. Sensitivity with variation in the cavity thickness in terms of (a) ΔI_{ON}, (b) ΔV_{TH}, (c) Δg_m, and (d) SS.

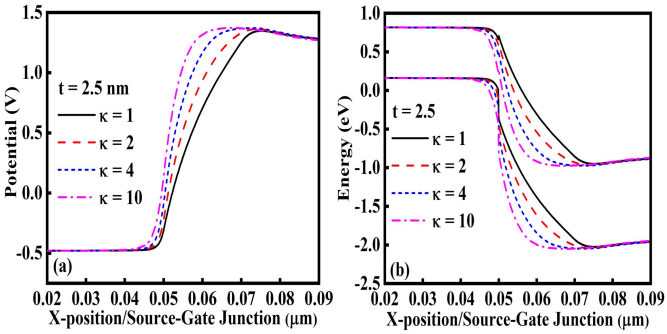

Fig. 5. (a) Potential and (b) energy band at Source-Gate Junction at 1 nm below oxide-silicon interface with dielectric constant variation in ON state ($V_{DS} = 1$ V; $V_{GS} = 2$ V) and cavity thickness is 2.5 nm.

$$\Delta V_{TH} = \left| V_{TH,\kappa} - V_{TH,air} \right| \tag{4}$$

$$\Delta g_m = \left| g_{m,\kappa} - g_{m,air} \right| \tag{5}$$

$\Delta\ I_{\rm ON}$, $\Delta\ V_{TH}$, and $\Delta\ g_m$ all three parameters increase with a decrease in cavity thickness. The SS decreases with an increase in the dielectric constant of the biomolecule. Thus, the reported biosensor with the cavity thickness of 2.5 nm shows the highest optimized sensitivity.

B. Dielectric Modulation Sensitivity for Cavity Thickness = 2.5 nm

The effects of dielectric constant variations of biomolecules with cavity thickness of 2.5 nm on the potential and energy band under oxide-silicon interface have been shown in Fig. 5 (a) and (b), respectively. With rise in the dielectric constant of biomolecules, gate capacitance will increase and the potential drop across the gate capacitance decreases and thus the potential under oxide-silicon interface increases as shown in Fig. 5 (a). This rise in the potential with an increase in the dielectric constant of biomolecules shifts the energy band downwards as illustrated in Fig. 5 (b), resulting in a shrinkage in the tunneling barrier and an improvement in the tunneling probability. This increase in the tunneling probability can also be depicted from equations (1) and (2) where an increase in ε_{bio} will lead to a decrease in tunneling length and thus increase in tunneling probability $T(E)$. Fig. 6 (a) shows

TABLE II
REPORTED BIOSENSOR SENSITIVITY COMPARISON WITH JLTFET BIOSENSOR

κ	Parameters	JLTFET [22]	Proposed
	V_{DS}	1.5 V	1 V
	V_{GS}	1.5 V	2 V
2	I_{ON} $(A/\mu m)$	2.70×10^{-8}	1.97103×10^{-8}
2	ΔI_{ON} $(A/\mu m)$	9.7×10^{-9}	1.96608×10^{-8}
10	I_{ON} $(A/\mu m)$	5.49×10^{-7}	3.34652×10^{-5}
10	ΔI_{ON} $(A/\mu m)$	5.317×10^{-7}	3.34652×10^{-5}

the transfer characteristics of the biosensor with variation in the dielectric constant of biomolecules. With an increase in the dielectric constant of biomolecules in the cavity, the tunneling length decreases and thus increases the probability of tunneling that leads to an increase in the drive current as evident from equation (1) and (2) and this variation in drive current can easily sense the biomolecules present. Fig. 6 (b) shows the transconductance of the biosensor with variation in the dielectric constant of biomolecules. Fig. 6 (c) shows absolute drain current sensitivity given as

$$\%Drain\ Current\ Sensitivity = \left| \frac{I_{D,\kappa} - I_{D,air}}{I_{D,air}} \times 100 \right| \tag{6}$$

Figure shows the % drain current sensitivity is in the range of 10^5 for $\kappa = 2$, 10^7 for $\kappa = 4$, and above 10^9 for $\kappa = 10$. This high sensitivity with variation in the dielectric constant of biomolecules will enable easy sensing.

Further, sensitivity in terms of $\Delta I_{\rm ON}$, ΔV_{TH} and Δg_m are given in equation (3), (4), and (5) and SS are shown in Fig. 6 (d) and (e), respectively. It shows an increase in sensitivity with increasing dielectric constant of biomolecules along with decrease in SS with an increase in dielectric constant. The sensitivity of reported biosensor is compared with existing JLFET biosensor and is found highly sensitive as evident by a brief perusal of Table. II.

C. Charge Density Modulation Sensitivity Analysis

Certain biomolecules exhibit charge density, hence the sensitivity analysis of such biomolecules must be done by charge density modulation. Here, analysis for the charge density variation from zero (neutral) to $1 \times 10^{12} cm^{-2}$ and from

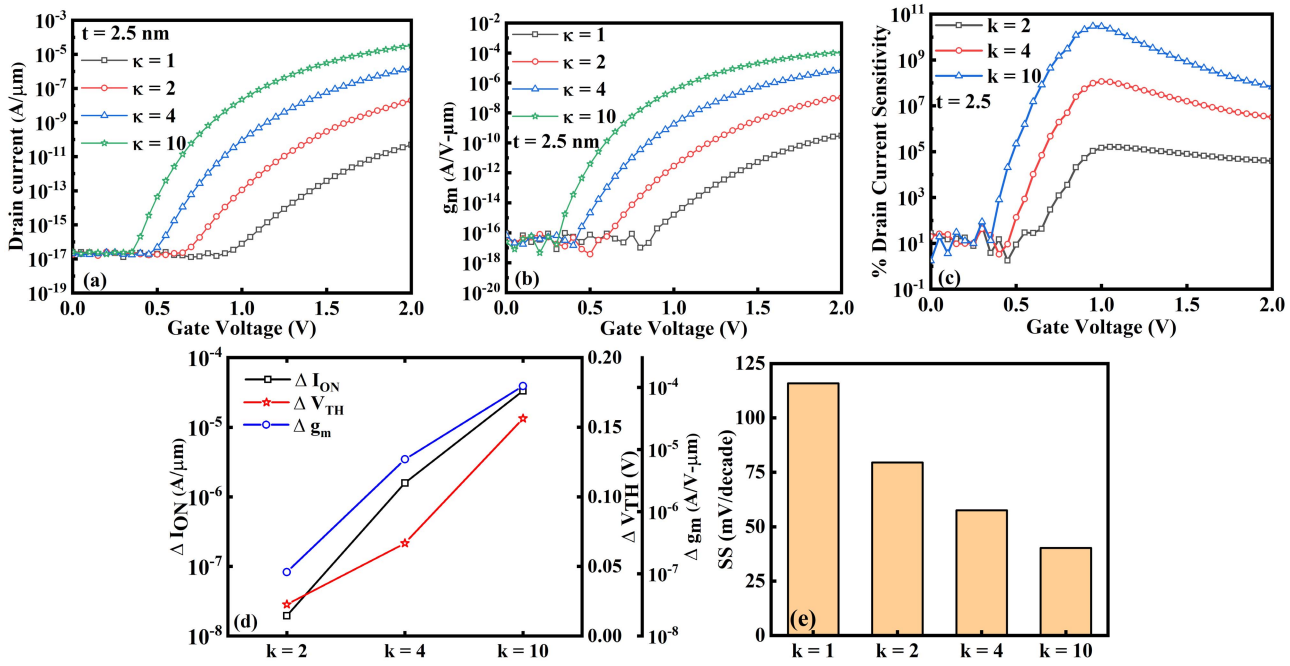

Fig. 6. (a) Transfer characteristics, (b) transconductance, (c) absolute drain current sensitivity (d) sensitivity in terms of ΔI_{ON}, ΔV_{TH}, and Δg_m and (e) SS with variation in dielectric constant of biomolecule in biosensor with cavity thickness 2.5 nm and $V_{DS} = 1$ V.

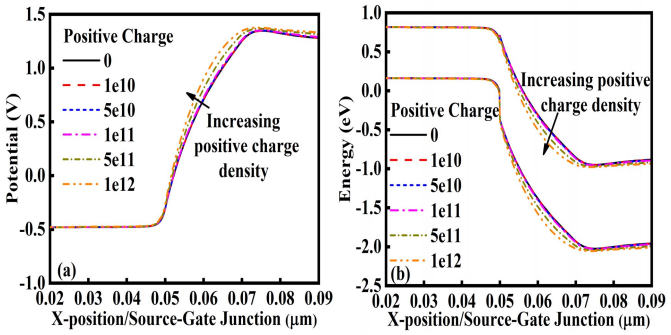

Fig. 7. (a) Potential and (b) energy band at source-gate junction 1 nm below oxide-silicon interface for variation in the positive charge density of biomolecules in ON state ($V_{DS} = 1$ V; $V_{GS} = 2$ V) and $\kappa = 1$.

zero (neutral) to $-1 \times 10^{12} cm^{-2}$ has been done. The effect on charge density on the flat band voltage and effective gate voltage can be expressed as [37]:

$$\Delta V_{fb} = \frac{q Q_f}{C_{eq}} \tag{7}$$

$$V_{GS_{eff}} = V_{GS} - V_{fb} \tag{8}$$

where, ΔV_{fb} is the change in flat band voltage, q is the electronic charge, Q_f is the charge density, C_{eq} is the equivalent capacitance of SiO_2 and biomolecules in the cavity.

The consequences of positive charge density variation from zero (neutral) to $1 \times 10^{12} cm^{-2}$ with dielectric constant 1 of biomolecule having the cavity thickness as 2.5 nm on the potential and energy band under oxide-silicon interface have been shown in Fig. 7 (a) and (b), respectively. With an increase in the positive charge density from zero (neutral) to $1 \times 10^{12} cm^{-2}$ of biomolecules the potential drop across the gate capacitance decreases and thus the potential under oxide-silicon interface increases as illustrated in Fig. 7 (a). This increase in the potential with an increase in positive charge density variation from zero (neutral) to 1×10^{12} of biomolecule shifts the energy band downwards as depicted in Fig. 7 (b), leading to a decrease in the tunneling barrier and an increase in the tunneling probability. This can further be explained by equations (7) and (8), flat band voltage decreases with an increase in the positive charge density and thus it increases the effective gate voltage. This increased effective gate voltage shifts the energy band in the channel region that leads to an increase in the energy range available for tunneling. Thus, it results in an increase in tunneling probability and drive current as depicted in equation (1). Fig. 8 (a) shows the transfer characteristics of the biosensor with positive charge density variation from zero (neutral) to $1 \times 10^{12} cm^{-2}$ with dielectric constant 1. It shows the drive current increases with an increase in positive charge density of biomolecules, this makes it easier to sense biomolecules based on the charge density present. Further, Fig. 8 (b) shows the transconductance and Fig. 8 (c) shows the sensitivity in terms of ΔI_{ON}, ΔV_{TH}, and Δg_m in presence of charged biomolecules can be calculated as,

$$\Delta I_{\text{ON}} = \left| I_{ON,charge} - I_{ON,neutral} \right| \tag{9}$$

$$\Delta V_{TH} = \left| V_{TH,charge} - V_{TH,neutral} \right| \tag{10}$$

$$\Delta g_m = \left| g_{m,charge} - g_{m,neutral} \right| \tag{11}$$

Fig. 8 (d) shows the variation in the SS with the variation in the positive charge of biomolecules. It shows an increase in the

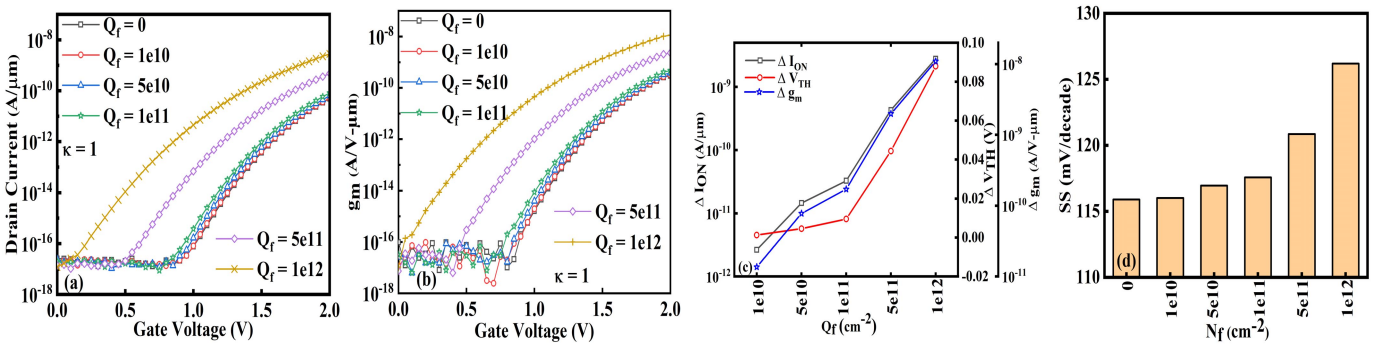

Fig. 8. (a) Transfer characteristics, (b) transconductance, (c) sensitivity in terms of $\Delta\ I_{ON}$, $\Delta\ V_{TH}$ and $\Delta\ g_m$, and (d) SS with variation in positive interface trap charge of biosensor with cavity thickness 2.5 nm and $V_{DS} = 1$ V.

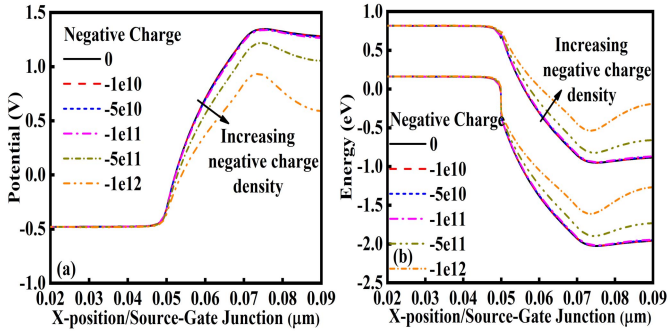

Fig. 9. (a) Potential and (b) energy band at source-gate junction at 1 nm below oxide-silicon interface for variation in the negative charge density of the biomolecules in ON state ($V_{DS} = 1$ V; $V_{GS} = 2$ V) and $\kappa = 1$.

sensitivity with an increase in the positive charge density of the biomolecules. The repercussions of negative charge density variation from zero (neutral) to $-1 \times 10^{12} cm^{-2}$ with dielectric constant as 1 for the biomolecule with cavity thickness 2.5 nm on the potential and energy band under oxide-silicon interface have been shown in Fig. 9 (a) and (b), respectively. With an increase in negative charge density from zero (neutral) to $-1 \times 10^{12} cm^{-2}$ of biomolecules the potential drop across the gate capacitance increases and thus the potential under oxide-silicon interface decreases as shown in Fig. 9 (a). This decrease in potential with an increase in the negative charge density variation from zero (neutral) to $-1 \times 10^{12} cm^{-2}$ of biomolecules shifts the energy band upwards as illustrated in Fig. 9 (b), leading to an increase in the tunneling barrier and a decrease in the tunneling probability. This can further be explained by equations (7) and (8), flat band voltage increases with an increase in the negative charge density and thus decreases the effective gate voltage. This decreased effective gate voltage shifts the energy band in the channel region leading to a decrease in the energy range available for the tunneling. Thus there is a decrease in the tunneling probability and drive current as governed by the equation (1). Fig. 10 (a) shows the transfer characteristics of biosensor with negative charge density variation from zero (neutral) to $-1 \times 10^{12} cm^{-2}$ with dielectric constant 1. It shows deterioration in drive current with rise in the negative charge density of the biomolecules, this makes it easier to sense biomolecules based on the charge density present. Further, Fig. 10 (b) shows the transconductance and Fig. 10 (c) shows the sensitivity in terms of $\Delta I_{\rm ON}$, ΔV_{TH}, and Δg_m as defined in equations (9), (10), and (11), respectively. Fig. 10 (d) shows the variation in SS with the variation in the negative charge of the biomolecules. It shows an increase in sensitivity with an increase in negative charge density of biomolecules. Further, the sensitivity of the reported biosensor is compared with [21]. It reveals that the reported biosensor is highly sensitive owing to its novel dual source, vertical channel device structure. It enables the biomolecules to be immobilized in both cavities above the source channel junctions, allowing it to modulate the tunneling length and energy range accessible for tunneling at both junctions.

D. Impact of Biomolecules Occupancy in Embedded Nanocavity on Drain Current

The embedded nanocavity formed for biomolecule immobilization is expected to be filled completely for biomolecule detection. However, in different biotests, it is observed that certain vacant spaces are present in the cavity region, which was expected to be fully filled with biomolecules. This appearance of vacant space in the cavity in different biotests will alter the electrical characteristics of the device from the expected characteristics. This contributes to another parameter for the sensitivity i.e. biomolecule occupancy ($\gamma\ Bio$) factor in the embedded nanocavity. $\gamma\ Bio$ represents the amount of cavity region filled with biomolecules (in %) and is described as

$$\gamma\ Bio = \frac{Thickness\ of\ cavity\ filled}{Total\ thickness\ of\ cavity\ (t_{cavity})} \times 100 \quad (12)$$

Fig. 11 shows transfer characteristics for the biosensor having cavity thickness as 2.5 nm and dielectric constant of 4 with the different biomolecules occupancy factors. Four different configurations of biomolecules occupancy have been analyzed i.e. 25 %, 50 %, 75 % and 100 %. For studying the effect of fill factor of the biomolecule in cavity, certain height of the cavity is filled with biomolecules and remaining is kept empty/filled with air. This variation in the biomolecules occupancy will vary the effective dielectric constant/capacitance of cavity region, an increase in biomolecules occupancy in cavity will increase effective dielectric constant/capacitance and thus

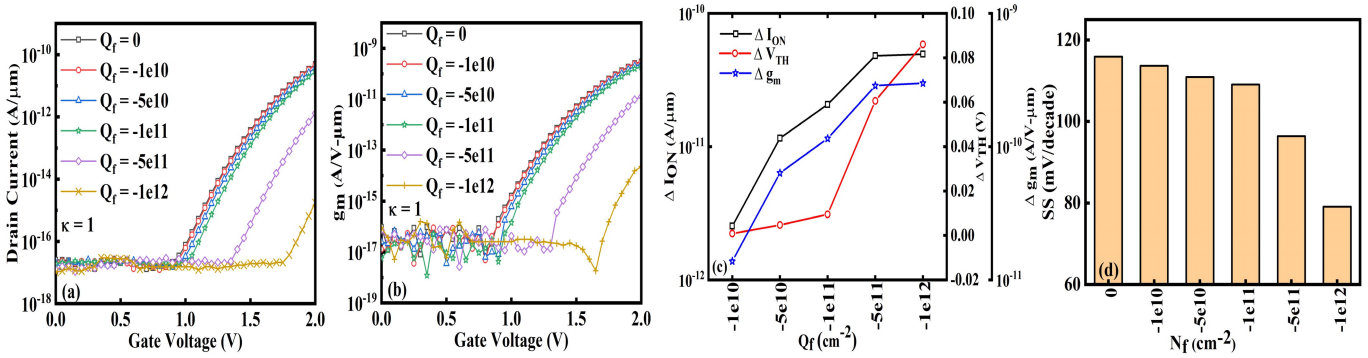

Fig. 10. (a) Transfer characteristics, (b) transconductance, (c) sensitivity in terms of $\Delta\, I_{ON}$, $\Delta\, V_{TH}$ and $\Delta\, g_m$, and (d) SS variations with variation in the negative charge density of biomolecules in the biosensor with cavity thickness 2.5 nm and $V_{DS} = 1$ V.

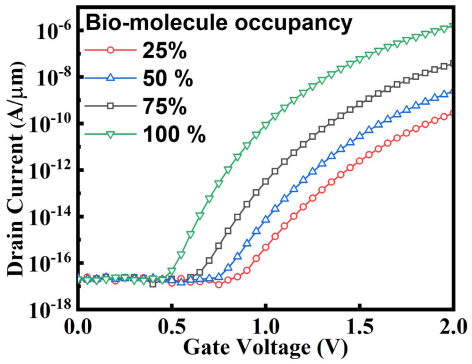

Fig. 11. Transfer characteristics variation with biomolecules occupancy in the cavity for the cavity thickness is 2.5 nm and dielectric constant of biomolecule is 4 at $V_{DS} = 1$ V.

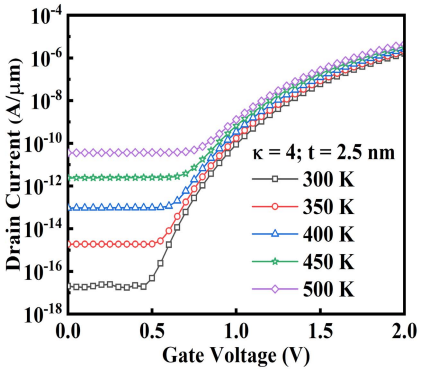

Fig. 12. Effect of temperature variations on reported biosensor with cavity thickness 2.5 nm and dielectric constant of biomolecules is considered as 4 at $V_{DS} = 1$ V.

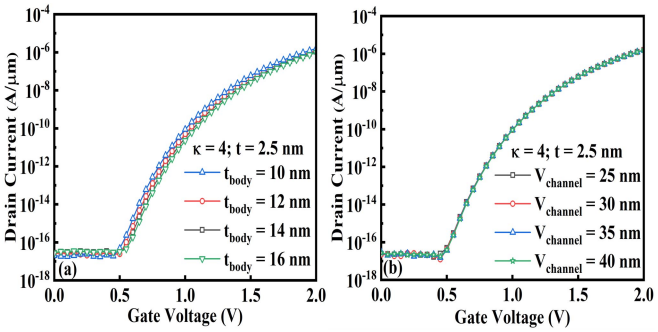

Fig. 13. (a) Effect of t_{body} variations and (b) effect of $V_{channel}$ variations on proposed biosensor with cavity thickness 2.5 nm and dielectric constant of biomolecules is considered as 4 at $V_{DS} = 1$ V.

will decrease the tunneling length causing improvement in the tunneling probability and drive current as expressed in equation (1) and (2).

With an increase in biomolecules occupancy in the cavity region from 25 % to 100 %. The gate capacitance increases thus there is an improvement in the drain current in ON state with improvement in biomolecules occupancy. Further, the reported biosensor is also highly resilient towards the process variations and temperature variations. The effects of process variation and temperature on the reported biosensor device structure are shown in the appendix section.

IV. Conclusion

This research article reports a vertically extended drain double gate $Si_{0.5}Ge_{0.5}$ source tunnel FET for the detection of the biomolecules such as cell, protein, DNA, etc. The reported biosensor features a dual source regions and two nanocavities at each source-channel junctions for the immobilization of biomolecules. This modulates the screening/tunneling length and energy range available for tunneling due to the changes in the dielectric constant and charge density variation of biomolecules. This dual cavity enhances the control of biomolecules on the source-channel tunneling probability and thus enhanced control on electrical performance parameters of the biosensor. It results in higher sensitivity of the biosensor towards the biomolecules. The biosensor sensitivity has been analyzed with respect to the dielectric constant and charge density modulation effects. The cavity length of 45 nm enables the detection of the large sized biomolecules and polymers. The ΔI_{ON} sensitivity of the reported biosensor for $\kappa = 2$ is $1.966 \times 10^{-8}\ A/\mu m$ and for $\kappa = 10$ is $3.34652 \times 10^{-5}\ A/\mu m$ with reference to air in the cavity.

Appendix

Fig. 12 shows the effect of temperature on biosensor characteristics, the graph shows change in current in the OFF state

whereas the current in the ON state is immune to temperature variations. As the biosensor sensitivity is studied in terms of ΔI_{ON}, ΔV_{TH}, and Δg_m. It can be inferred that the sensitivity of the biosensor is immune to temperature variations. Further, Fig.13 (a) and (b) show the effect of process variations on device characteristics, i.e. with variation in t_{body} and $V_{channel}$, respectively. The characteristics depict that the reported device structure is also immune towards the process variations.

REFERENCES

[1] S. O. Koswatta, M. S. Lundstrom, and D. E. Nikonov, "Performance comparison between p-i-n tunneling transistors and conventional MOSFETs," *IEEE Trans. Electron Devices*, vol. 56, no. 3, pp. 456–465, Mar. 2009.

[2] K. Boucart, W. Riess, and A. M. Ionescu, "Lateral strain profile as key technology booster for all-silicon tunnel FETs," *IEEE Electron Device Lett.*, vol. 30, no. 6, pp. 656–658, Jun. 2009.

[3] Q. Zhang, W. Zhao, and A. Seabaugh, "Low-subthreshold-swing tunnel transistors," *IEEE Electron Device Lett.*, vol. 27, no. 4, pp. 297–300, Apr. 2006.

[4] W. Y. Choi, B.-G. Park, J. D. Lee, and T.-J. K. Liu, "Tunneling field-effect transistors (TFETs) with subthreshold swing (SS) less than 60 mV/dec," *IEEE Electron Device Lett.*, vol. 28, no. 8, pp. 743–745, Aug. 2007.

[5] S. W. Kim, J. H. Kim, T.-J. K. Liu, W. Y. Choi, and B.-G. Park, "Demonstration of L-shaped tunnel field-effect transistors," *IEEE Trans. Electron Devices*, vol. 63, no. 4, pp. 1774–1778, Apr. 2016.

[6] S. Saurabh and M. J. Kumar, "Novel attributes of a dual material gate nanoscale tunnel field-effect transistor," *IEEE Trans. Electron Devices*, vol. 58, no. 2, pp. 404–410, Feb. 2011.

[7] Y. Khatami and K. Banerjee, "Steep subthreshold slope n- and p-type tunnel-FET devices for low-power and energy-efficient digital circuits," *IEEE Trans. Electron Devices*, vol. 56, no. 11, pp. 2752–2761, Nov. 2009.

[8] A. Vladimirescu, A. Amara, and C. Anghel, "An analysis on the ambipolar current in Si double-gate tunnel FETs," *Solid-State Electron.*, vol. 70, pp. 67–72, Apr. 2012.

[9] M. R. U. Shaikh and S. A. Loan, "Drain-engineered TFET with fully suppressed ambipolarity for high-frequency application," *IEEE Trans. Electron Devices*, vol. 66, no. 4, pp. 1628–1634, Apr. 2019.

[10] G. B. Beneventi, E. Gnani, A. Gnudi, S. Reggiani, and G. Baccarani, "Can interface traps suppress TFET ambipolarity?" *IEEE Electron Device Lett.*, vol. 34, no. 12, pp. 1557–1559, Dec. 2013.

[11] A. Raj, S. Singh, K. N. Priyadarshani, R. Arya, and A. Naugarhiya, "Vertically extended drain double gate $Si_{1-x}Ge_x$ source tunnel FET: Proposal & investigation for optimized device performance," *Silicon*, pp. 1–16, Jul. 2020.

[12] K. Vanlalawpuia and B. Bhowmick, "Investigation of a Ge-source vertical TFET with delta-doped layer," *IEEE Trans. Electron Devices*, vol. 66, no. 10, pp. 4439–4445, Oct. 2019.

[13] D. Sarkar and K. Banerjee, "Fundamental limitations of conventional-FET biosensors: Quantum-mechanical-tunneling to the rescue," in *Proc. 70th Device Res. Conf.*, Jun. 2012, pp. 83–84.

[14] P. Bergveld, "Development of an ion-sensitive solid-state device for neurophysiological measurements," *IEEE Trans. Biomed. Eng.*, vol. BME-17, no. 1, pp. 70–71, Jan. 1970.

[15] H. Im, X.-J. Huang, B. Gu, and Y.-K. Choi, "A dielectric-modulated field-effect transistor for biosensing," *Nature Nanotechnol.*, vol. 2, pp. 430–434, Jul. 2007.

[16] C.-H. Kim, C. Jung, H. G. Park, and Y.-K. Choi, "Novel dielectric modulated field-effect transistor for label-free DNA detection," *Biochip J.*, vol. 2, no. 2, pp. 127–134, 2008.

[17] P. Dwivedi and A. Kranti, "Dielectric modulated biosensor architecture: Tunneling or accumulation based transistor?" *IEEE Sensors J.*, vol. 18, no. 8, pp. 3228–3235, Apr. 2018.

[18] R. Narang, M. Saxena, and M. Gupta, "Comparative analysis of dielectric-modulated FET and TFET-based biosensor," *IEEE Trans. Nanotechnol.*, vol. 14, no. 3, pp. 427–435, May 2015.

[19] S. Kanungo, S. Chattopadhyay, P. S. Gupta, and H. Rahaman, "Comparative performance analysis of the dielectrically modulated full-gate and short-gate tunnel FET-based biosensors," *IEEE Trans. Electron Devices*, vol. 62, no. 3, pp. 994–1001, Mar. 2015.

[20] R. Narang, M. Saxena, R. S. Gupta, and M. Gupta, "Dielectric modulated tunnel field-effect transistor—A biomolecule sensor," *IEEE Electron Device Lett.*, vol. 33, no. 2, pp. 266–268, Feb. 2012.

[21] G. Wadhwa and B. Raj, "Design, simulation and performance analysis of JLTFET biosensor for high sensitivity," *IEEE Trans. Nanotechnol.*, vol. 18, pp. 567–574, May 2019.

[22] G. Wadhwa and B. Raj, "Parametric variation analysis of symmetric double gate charge plasma JLTFET for biosensor application," *IEEE Sensors J.*, vol. 18, no. 15, pp. 6070–6077, Aug. 2018.

[23] P. Yang, H. Rong, Z. Wu, and Y. Pei, "Biosensor based on In_2O_2 electrolyte gated thin film transistor with integrated on-chip gate electrode," *IEEE Trans. Nanobiosci.*, vol. 20, no. 3, pp. 287–290, Jul. 2021.

[24] U. Kasiviswanathan *et al.*, "Aluminium oxide thin-film based *in vitro* cell-substrate sensing device for monitoring proliferation of myoblast cells," *IEEE Trans. Nanobiosci.*, vol. 20, no. 3, pp. 331–337, Jul. 2021.

[25] N. Ayyanar, K. V. Sreekanth, G. T. Raja, and M. S. M. Rajan, "Photonic crystal fiber-based reconfigurable biosensor using phase change material," *IEEE Trans. Nanobiosci.*, vol. 20, no. 3, pp. 338–344, Jul. 2021.

[26] *ATLAS Device Simulation Software*, Silvaco Int., Santa Clara, CA, USA, 2013.

[27] K. Boucart and A. M. Ionescu, "Double-gate tunnel FET with high-κ gate dielectric," *IEEE Trans. Electron Devices*, vol. 54, no. 7, pp. 1725–1733, Jul. 2007.

[28] P. M. Solomon *et al.*, "Universal tunneling behavior in technologically relevant P/N junction diodes," *J. Appl. Phys.*, vol. 95, no. 10, pp. 5800–5812, 2004.

[29] R. Pillarisetty *et al.*, "High mobility strained germanium quantum well field effect transistor as the p-channel device option for low power ($V_{cc} = 0.5$ V) III–V CMOS architecture," in *IEDM Tech. Dig.*, Dec. 2010, pp. 6–7.

[30] T. Tezuka, N. Sugiyama, and S. Takagi, "Fabrication of strained Si on an ultrathin SiGe-on-insulator virtual substrate with a high-Ge fraction," *Appl. Phys. Lett.*, vol. 79, no. 12, pp. 798–1800, 2001.

[31] T.-Y. Liow *et al.*, "Investigation of silicon-germanium fins fabricated using germanium condensation on vertical compliant structures," *Appl. Phys. Lett.*, vol. 87, no. 26, Dec. 2005, Art. no. 262104.

[32] S. Balakumar *et al.*, "Germanium-rich SiGe nanowires formed through oxidation of patterned SiGe FINs on insulator," *J. Electron. Mater.*, vol. 38, no. 3, pp. 443–448, Mar. 2009.

[33] Y. Jiang *et al.*, "Ge-rich (70%) SiGe nanowire MOSFET fabricated using pattern-dependent Ge-condensation technique," *IEEE Electron Device Lett.*, vol. 29, no. 6, pp. 595–598, Jun. 2008.

[34] A. Paliwal, M. Tomar, and V. Gupta, "Complex dielectric constant of various biomolecules as a function of wavelength using surface plasmon resonance," *J. Appl. Phys.*, vol. 116, no. 2, pp. 23101–23109, Jul. 2014.

[35] A. Densmore *et al.*, "Spiral-path high-sensitivity silicon photonic wire molecular sensor with temperature-independent response," *Opt. Lett.*, vol. 33, pp. 596–598, Mar. 2008.

[36] E. Makarona *et al.*, "Vertical devices of self-assembled hybrid organic/inorganic monolayers based on tungsten polyoxometalates," *Microelectron. Eng.*, vol. 85, nos. 5–6, pp. 1399–1402, May 2008.

[37] P. Kumari, A. Raj, K. N. Priyadarshani, and S. Singh, "Impact of temperature and interface trapped charges variation on the analog/RF and linearity of vertically extended drain double gate $Si_{0.5}Ge_{0.5}$ source tunnel FET," *Microelectron. J.*, vol. 113, Jul. 2021, Art. no. 105077.